STREAMFLOW SIMULATION BASED ON LAND USE/COVER CHANGE USING INTEGRATED GOOGLE EARTH ENGINE AND SWAT+ IN AN AGRICULTURE-DOMINATED BASIN, NORTHEAST THAILAND

Isared Kakarndee[1] Pattara Rirugchart[2*] Nuantip Chaladlert[3] Pongsak Jindasee[4]

Received : March 18,2025
Revised : June 11, 2025
Accepted : June 30, 2025

Abstract

Streamflow is a fundamental component of the hydrological cycle, and land use/land cover (LULC) significantly influences runoff processes. This study investigates the impacts of Land Use and Land Cover Change (LUCC) on streamflow in the Upper Songkhram River Basin (USRB), Northeast Thailand using Google Earth Engine (GEE) and the SWAT+ hydrological model. GEE facilitated high accuracy LULC classification (overall accuracy: 83-91%, Kappa coefficient: 0.76-0.85), revealing a marked increase in para rubber plantations and built-up areas, and a decrease in paddy fields and forests between 2003 and 2023. The calibrated and validated SWAT+ model (NSE: 0.86/0.79, R^2: 0.91/0.89, PBIAS: -24.5%/-36.7%) simulated the streamflow changes associated with LUCC. Results indicate a substantial increase in wet season streamflow, particularly in August (28.9 m^3/s) and September (25.6 m^3/s), primarily due to the decline of paddy fields and their water retention capacity. This study emphasizes the link between land use and hydrology, showcasing the combined utility of GEE and SWAT+ for assessing LUCC impacts. These findings offer valuable insights for sustainable water resource management and land use planning in Thailand and comparable regions worldwide.

Keywords: Google Earth Engine, LULC change, Northeast Thailand, Streamflow, SWAT+

[1] Department of Farm Mechanics, Faculty of Agriculture, Kasetsart University, e-mail: isared.k@ku.th
[2] Department of Geography, Faculty of Social Sciences, Srinakharinwirot University, e-mail: pattara.rirugchart@g.swu.ac.th
[3] Hydro – Informatics Institute, e-mail: nuantip@hii.or.th
[4] Hydro – Informatics Institute, e-mail: pongsak@hii.or.th.
** Corresponding author, e-mail : pattara.rirugchart@g.swu.ac.th*

Introduction

Land Use and Land Cover Change (LUCC) significantly alters Earth hydrological cycle, affecting precipitation, infiltration, evapotranspiration, and runoff (Petchprayoon et al., 2010; Yong et al., 2012). The consequences include increased flooding, soil erosion, and reduced groundwater availability (Zope et al., 2014). Understanding the link between LUCC and hydrology is crucial for proactive water resource management (Näschen et al., 2019; Guo et al., 2020). Extensive research underscores these LUCC-induced hydrological impacts. Deforestation can increase river discharge and modify seasonal water flows (Luo et al., 2016), while rapid land-use changes in Asia threaten water resources (Peng et al., 2023). Thailand exemplifies how LUCC interacts with localized factors like topography and climate to affect hydrology (Kim et al., 2005; Petchprayoon et al., 2010).

However, the key drivers of LUCC influencing the hydrological cycle at the watershed scale have yet to be systematically analyzed, particularly in the region-specific context of Thailand. This limitation hinders the availability of accurate and up-to-date data to support spatially explicit water resource management. A critical water management challenge is to evaluate which specific land-use changes most significantly affect streamflow regimes over the long term. Such information is essential for planning flood prevention, soil and water conservation, and sustainable groundwater resource management.

Satellite imagery has revolutionized Earth surface observations, particularly in geographically inaccessible regions and areas lacking comprehensive ground-based surveys (Hansen et al., 2013; Gorelick et al., 2017). The European Space Agency's Sentinel-2 satellite system provides high-resolution multispectral imagery that has proven instrumental for land use and land cover (LULC) analysis, demonstrating classification accuracy exceeding 81% through the implementation of advanced machine learning algorithms (Ninad, 2024). A methodological transition from pixel-based to object-based classification approaches has significantly enhanced LULC precision, facilitating both change detection and resource management initiatives (Ara et al., 2023). Contemporary remote sensing technologies, including microwave and hyperspectral imaging systems, have further augmented data acquisition capabilities and spatial resolution, enabling effective mapping under challenging environmental conditions (Mbinya Manetu et al., 2023). Moreover, recent advancements in geomatics techniques have substantially improved satellite image resolution for precise surveying applications (Kadhum et al., 2023), thereby supporting evidence-based sustainable land management practices (Lozano and Regan, 2018).

In the context of Thailand, where field data and spatial survey resources are limited in certain regions, remote sensing technology offers a high potential to monitor LUCC and support evidence-based natural resource planning.

Accurately analyzing LUCC necessitates cutting-edge tools like remote sensing and GIS (Huang et al., 2017). Google Earth Engine (GEE) offers free satellite imagery and cloud-based processing, streamlining LUCC assessments (Gorelick et al., 2017). GEE facilitates large-scale LUCC analysis, aids hydrological modeling, and supports the integration of land cover data into models like SWAT for water resource impact assessment (Abbaspour et al., 2015; Gorelick et al., 2017; Younes et al., 2023). SWAT, a well-established hydrological model, and its enhanced version SWAT+ (Bieger et al., 2017; Kakarndee & Kositsakulchai, 2020), allow for refined simulations (Gassman et al., 2007; Zhang et al., 2022).

Nevertheless, previous studies have typically applied GEE and SWAT independently, despite the considerable advantages of these platforms. The combined effect between GEE and SWAT+ enables efficient satellite data processing through GEE's cloud infrastructure, directly linking high-resolution spatial data with SWAT+'s advanced hydrological modeling capabilities. This integration enhances spatial-temporal resolution, facilitates multi-year analyses, and allows scenario-based assessments reflecting Thailand's complex watershed conditions. This gap in current knowledge highlights the need for comprehensive application of integrated GEE-SWAT+ frameworks for watershed-scale studies in Thailand.

This research aims to use GEE to identify LUCC drivers and model potential hydrological outcomes using SWAT+. It will investigate the impact of specific land-use changes (e.g., deforestation, agricultural expansion) on streamflow patterns. The primary research questions are: 1) Which land-use changes significantly influence hydrological responses within the study watershed? 2) How accurately can the combined use of GEE and SWAT+ predict hydrological impacts at the watershed scale? 3) What sustainable water management strategies can be formulated based on modeled outcomes under various future land-use scenarios?

The study outcomes propose to provide data-driven water management guidelines, including zoning for conservation, land-use regulation, and watershed restoration strategies to maintain water security within the study area. Furthermore, the developed framework and tools will be adaptable for application in other watersheds exhibiting similar geographic and LUCC characteristics.

Materials and methods

Study area

The Upper Songkhram River Basin (USRB), located in Northeast Thailand, encompasses an area of approximately 3,300 km² (Figure 1). Situated between 16°54′ – 18°23′ latitude and 103°10′ – 104°29′ longitude, the basin drains into the Mekong River. Its elevation ranges from 135 to 675 meters above mean sea level (masl) (Muangthong & Shrestha, 2015). Originating in

the Western Phu Phan Mountains, the USRB flows through five provinces: Udon Thani, Sakon Nakhon, Nong Khai, and Bueng Kan. In recent decades, extensive deforestation and the widespread conversion of paddy fields into para rubber plantations have significantly altered the basin's hydrodynamics. Paddy fields, which previously functioned as natural flood buffers, have been replaced by less permeable or water-retentive land uses, exacerbating flood risks during the monsoon season (Chotpantarat & Boonkaewwan, 2018).

Data

This study uses freely available satellite images from Google Earth Engine (GEE) to map changes in land use and land cover (LULC). Imagery from three Landsat satellites Landsat 7 ETM+ (2003), Landsat 8 (OLI TIRS) (2013), and the newest Landsat 9 OLI 2 (2023) were analyzed. The process of accessing these large datasets was greatly simplified by the cloud computing platform within GEE. Additionally, data from Open Street Map and DMSP OLS were incorporated to strengthen our analysis. To set up a SWAT+ model for this study, data was gathered from various sources. A 90-meter resolution digital elevation model (DEM), downloaded from www.earthdata.nasa.gov/data/instruments/srtm, was used to define watershed boundaries, drainage patterns, slopes, and landscape units with streams and rivers.

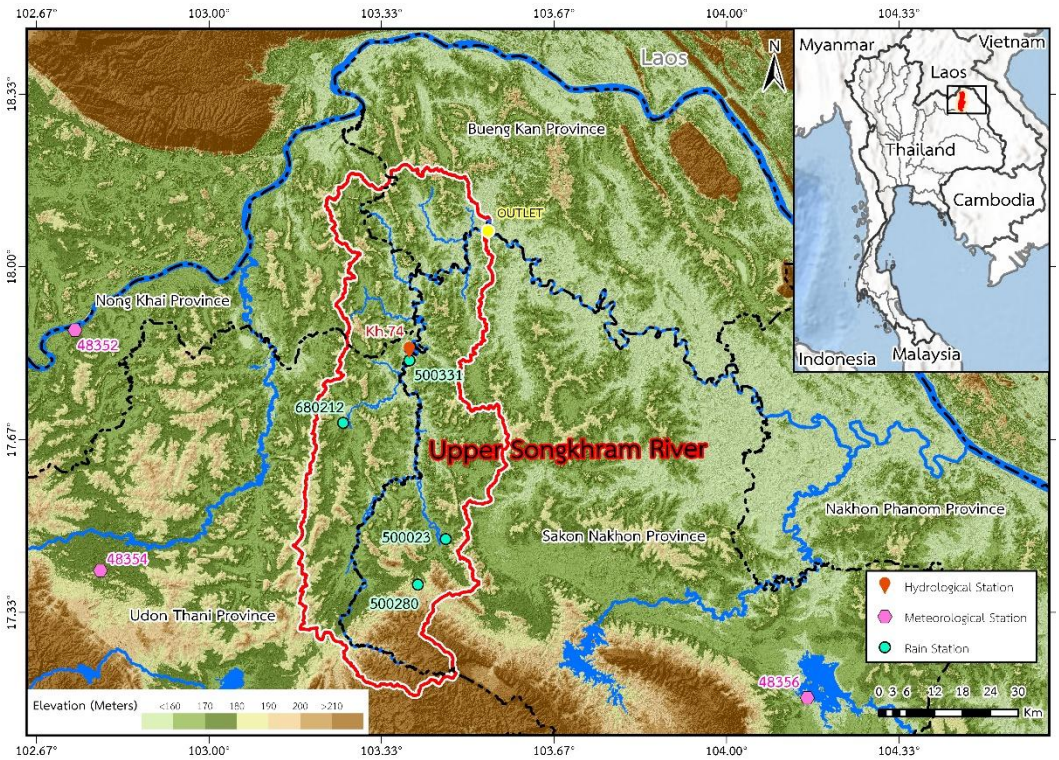

Figure 1 The Upper Songkhram River Basin (URSB)

Land use and soil maps, along with soil properties provided by the Land Development Department (LDD), were utilized to create hydrological response units (HRUs). Daily climate data (humidity, temperature, sunshine, and wind speed) was obtained from Nong Khai (48352) and Udon Thani (48354) stations (Figure 1) of the Thai Meteorological Department (TMD) to simulate streamflow within the watershed for the period of 2014 to 2022. Finally, observed flow measurements from the Kh.74 station, recorded by the Royal Irrigation Department (RID) over the same period, were employed to calibrate and validate the model accuracy.

Google Earth Engine

Google Earth Engine (GEE) (Figure 2), a cloud-based geospatial analysis platform launched by Google in 2010, has significantly evolved to become a powerful tool for Earth observation and geospatial analysis (Gorelick et al., 2017). It provides access to a vast archive of satellite imagery and analytical tools, revolutionizing research by enabling large-scale environmental monitoring and planetary analysis (Velastegui-Montoya et al., 2023). Initially designed for remote sensing applications, GEE has expanded its capabilities to support land cover classification (Hansen et al., 2013), deforestation monitoring (Tyukavina et al., 2018), and hydrological modeling (Tamiminia et al., 2020; Alzurqani et al., 2024). The integration of machine learning and big data analytics has further enhanced its role in climate change studies (Amani et al., 2020) and precision agriculture (Shelestov et al., 2017). GEE offers a web interface for scripting, data exploration, and programmatic access via Python and JavaScript libraries (Gorelick et al., 2017). Recent advancements have focused on improving computational efficiency and accessibility, making it an indispensable resource for researchers and policymakers worldwide (Mutanga & Kumar, 2019). In this study, a GEE script was developed to perform remote sensing analysis by importing a watershed boundary (SBasin) as a FeatureCollection and extracting its geometry for spatial filtering. The script defines a time range (January to December 2023) and selects Sentinel-2 bands relevant for bands B2, B3, B4, B8, B11, and B12 relevant for vegetation and land analysis. It loads the Sentinel-2 surface reflectance image collection, filters it by date and study area, and excludes images with more than 10% cloud cover. A median composite image is then generated to reduce noise caused by clouds and temporal variability. Subsequently, the Normalized Difference Vegetation Index (NDVI) is calculated using the near-infrared (B8) and red (B4) bands to assess vegetation health. Finally, the map is centered on the watershed and the NDVI result is displayed as a visual layer for interpretation.

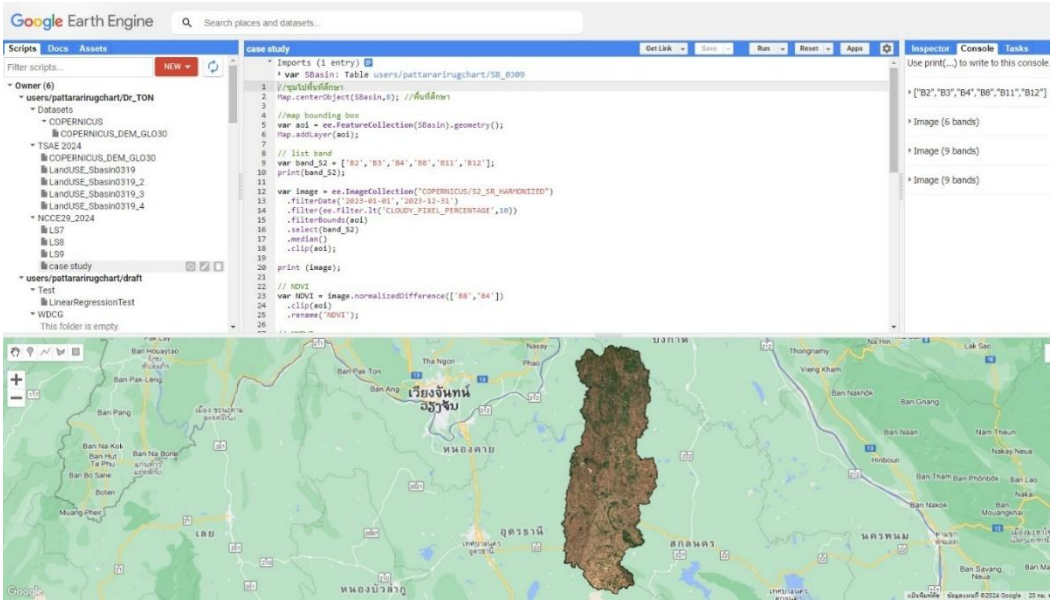

Figure 2 Google Earth Engine Platform Interface

Soil & Water Assessment Tool Plus

The Soil & Water Assessment Tool Plus (SWAT+) advances watershed modeling by refining stream and topography mapping beyond its predecessor, SWAT (Bieger et al., 2017; Her & Jeong, 2018). This freely available tool (https://swat.tamu.edu/software/plus/) simulates surface and groundwater dynamics, facilitating the assessment of environmental impacts related to land use, agriculture, and climate change (Williams et al., 2010; Gassman et al., 2014).

Originally developed in the early 1990s as an extension of previous USDA models, the Soil & Water Assessment Tool (SWAT) simulates the impacts of land management on water, sediment, and agricultural chemical yields in large watersheds (Arnold et al., 2007). Over time, SWAT has been widely used and enhanced with better hydrological, soil, and climate modeling capabilities. To address the need for improved spatial representation and modular flexibility, SWAT+ was introduced as an upgraded version. It allows for more detailed representation of landscape units, flexible connectivity between hydrological features, and improved management simulations (Bieger et al., 2017). SWAT+ enhances the original model by incorporating refined spatial discretization, enabling more precise analysis of hydrological processes and human interventions on water resources (Kakarndee & Kositsakulchai, 2020; Wu et al., 2020; Čerkasova et al., 2023). Recent studies have leveraged SWAT+ for more detailed watershed-scale modeling, integrating advanced remote sensing and machine learning

techniques to improve prediction accuracy and decision-making in water resource management (Woo et al., 2019; Qi et al., 2024).

The complexity of the model structure requires new users to spend a significant amount of time learning and understanding the system. Additionally, SWAT+ relies on high-resolution input data, which may be difficult to obtain in certain regions, especially in developing countries. Moreover, the processes of model calibration and validation remain time-consuming and resource intensive. Although SWAT+ features a modular architecture, its integration with external tools such as GIS or land use change models still demands technical expertise and domain-specific knowledge.

Model performance evaluation

Model performance was evaluated using three statistical criteria: Nash-Sutcliffe Efficiency (NSE) (Eq. 1) to assess the agreement between simulations and observations, the Coefficient of Determination (R^2) (Eq. 2) to measure the strength of the linear relationship, and Percent Bias (PBIAS) (Eq. 3) to quantify systematic bias. All performance indicators achieved statistically significant values during calibration and validation, meeting the established criteria outlined by Abbaspour et al. (2007).

$$NSE = 1 - \left(\sum_{i=1}^{n} (\mathrm{O}_i - P_i)^2 \Big/ \sum_{i=1}^{n} (\mathrm{O}_i - \overline{O}_i)^2 \right) \qquad (1)$$

$$r^2 = \left[\frac{\sum_{i=1}^{n} \left[(\mathrm{O}_i - \overline{O}_i)(\mathrm{P}_i - \overline{P}_i) \right]}{\left[\sum_{i=1}^{n} (\mathrm{O}_i - \overline{O}_i)^2 \right]^{0.5} \left[\sum_{i=1}^{n} (\mathrm{P}_i - \overline{P}_i)^2 \right]^{0.5}} \right]^2 \qquad (2)$$

$$PBIAS = \left(\sum_{i=1}^{n} O_i - \sum_{i=1}^{n} P_i \Big/ \sum_{i=1}^{n} O_i \right) \times 100 \qquad (3)$$

where Q is the observed flow, $\overline{Q}$ is the mean of the observed flow, P is the simulated flow, $\overline{P}$ is the mean of the simulated flow, and all unit data is in m^3/s.

Methodology

For this study, a three-step approach (Figure 3) is used to process the impact of land-use and land-cover (LULC) change on streamflow in the USRB. The analysis employs the SWAT+ model and LULC maps generated by GEE.

First, Landsat imagery (2003, 2013, 2023) from Google Earth Engine (GEE) is classified using supervised machine learning (e.g., Random Forest) to generate LULC maps (Sain, 1996; Breiman, 2001). Training data, including field observations and secondary data from the Land Development Department (LDD), ensures accuracy, which is then assessed using the Kappa coefficient (Congalton, 1991). Classification accuracy is evaluated based on error values from the Error Matrix, alongside overall accuracy (Wafdan, 2021). Both metrics should ideally fall between 85-95% (Anderson et al., 1976). The error matrix (or confusion matrix) is a table that compares predicted classes with actual classes, showing how well a classification model performs. The Kappa coefficient (**K**) measures the level of agreement between the predicted and actual classifications, adjusting for chance agreement. It is calculated using the formula **K** = (Po – Pe) / (1 – Pe), where Po is the observed agreement (proportion of correctly classified cases) and Pe is the expected agreement by chance based on row and column totals in the matrix.

Second, the SWAT+ model setup incorporates DEM, LULC, soil maps, and daily climate data (2014–2023). The observed streamflow data is used for model calibration (2014–2017) and validation (2018–2021). The model setup begins with watershed delineation using the DEM, followed by the definition of Hydrologic Response Units (HRUs) based on the combination of land use, soil type, and slope class. Initial parameter values are assigned based on literature and default SWAT+ databases. For model calibration and validation, the SWAT+ Toolbox (Chawanda, 2022), a free software tool (https://celray.github.io/SWATPlusToolbox/3.0.3/), is utilized for sensitivity analysis and parameter optimization specifically for SWAT+. The performance of the model during calibration (2014–2017) and validation (2018–2021) is assessed using performance indices such as NSE, R^2, and PBIAS. These metrics ensure agreement between simulated and observed streamflow, following the criteria suggested by (Abbaspour et al., 2007).

Finally, the streamflow was simulated using different LULC maps derived from GEE for the years 2003, 2013, and 2023, utilizing the climate dataset from 2014 to 2018. The comparisons were made separately for the dry period (November–April) and the wet period (May–October). This approach enables an analysis of streamflow changes and the impact of LULC alterations on hydrological responses. The calibration of the SWAT+ model focused on key parameters identified through sensitivity analysis. The Curve Number for moisture condition II (CN2) was adjusted within a relative range of -0.15 to -0.05, while the baseflow alpha factor (ALPHA_BF) was calibrated between 0.1 and 0.4 days. Groundwater delay time (GW_DELAY) varied from 15 to 60 days, and the threshold depth of water in the shallow aquifer for return flow (GWQMN)

ranged from 100 to 500 mm. Soil-related parameters such as saturated hydraulic conductivity (SOL_K) and available water capacity (SOL_AWC) were also optimized, with SOL_K ranging from 2 to 50 mm/hr depending on the HRU, and SOL_AWC from 0.10 to 0.25 based on soil type.

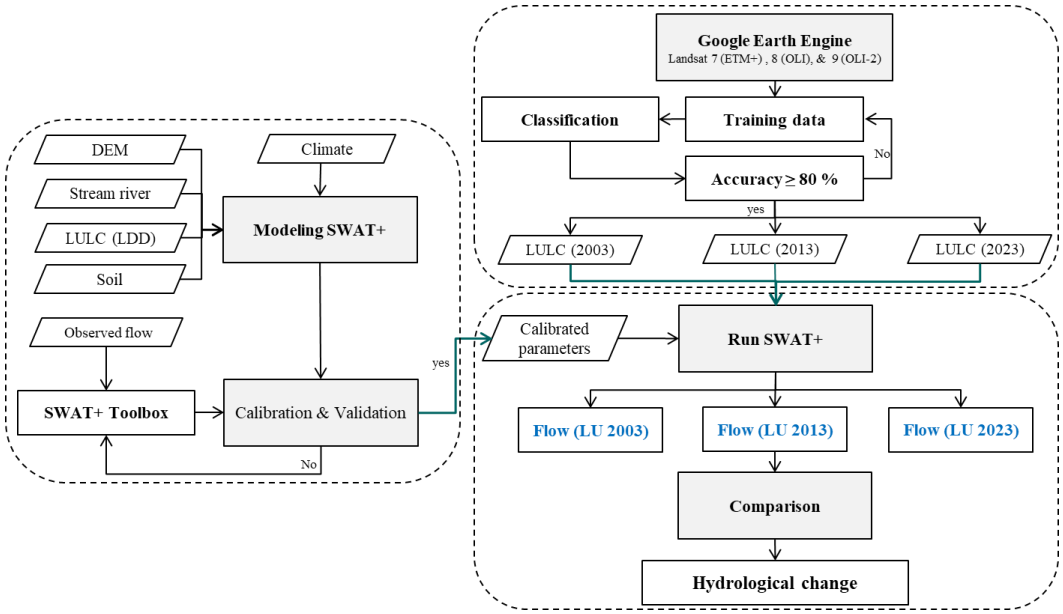

Figure 3 Flowchart of the Research Methodology

Results and discussion

LUILC classification and accuracy assessment

The USRB LULC classification identifies seven land use types: paddy fields, agricultural land, sugarcane, para rubber, forests, built-up areas, and water (as shown in Table 1 and Figure 4). LULC classifications for 2003, 2013, and 2023 (Figure 4) demonstrated high accuracy levels. In 2003, overall accuracy was 88.18% (Kappa coefficient: 0.81), improving to 91.02% (Kappa: 0.85) in 2013. The 2023 classification had an overall accuracy of 83.56% (Kappa: 0.76), indicating a robust methodology for mapping LULC patterns within the study area.

Table 1 presents the LULC changes within the USRB from 2003 to 2023. It reveals a decrease of 464.31 km² in paddy fields, while agricultural land increased by 358.98 km². The sugarcane plantations decreased, whereas para rubber plantations expanded by 886.59 km², the largest increase among the LULC types. Forest areas decreased by 129.51 km², while built-up areas expanded by 74.57 km², the second-largest increase, following the growth of water resource, which increased by 25.32 km².

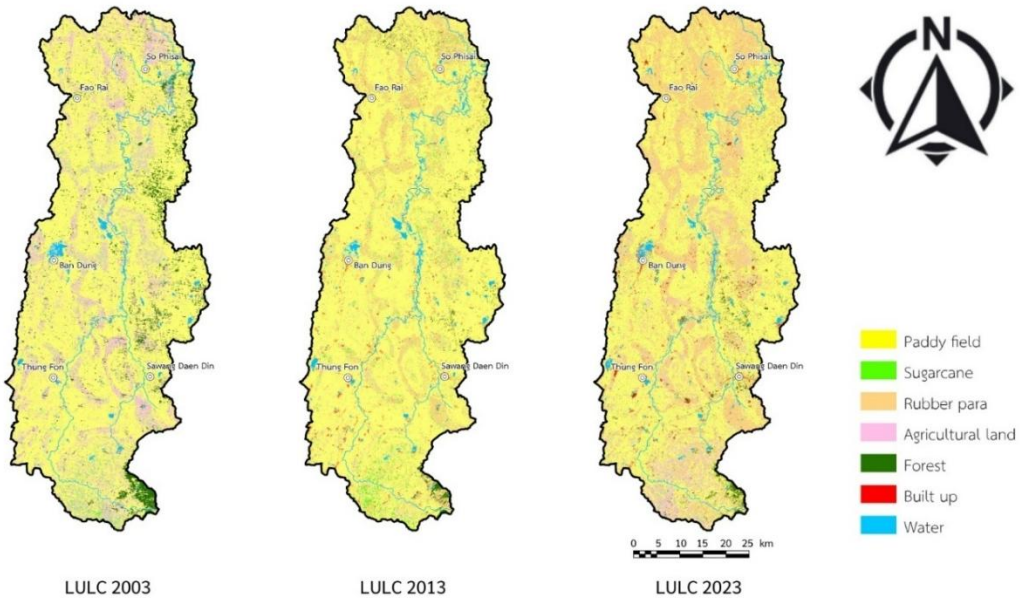

Figure 4 Land Use and Land Cover (LULC) maps for the years 2003, 2013, and 2023

Table 1 LULC classification of land use for the years 2003, 2013, and 2023

LULC types	Area (km²)		
	LULC 2003	LULC 2013	LULC 2023
1. Paddy field	2,397.3	2,533.7	1,932.9
2. Agriculture	544.7	85.7	185.7
3. Sugarcane	83.7	87.1	50.1
4. Para rubber	0.4	396.9	886.9
5. Forest	210.1	66.1	80.6
6. Built up	10.3	61.6	84.8
7. Water	41.3	56.8	66.6

The analysis of four agricultural sector types (paddy fields, agricultural land, sugarcane, and para rubber) reveals significant changes in land use patterns over time. In 2003, rubber plantations covered only a small area due to their limited popularity, with most of the land being dedicated to other agricultural sectors. However, by 2013, rubber plantations experienced rapid expansion, reaching nearly 400 km². In contrast, other agricultural sectors saw considerable

declines during this period. This trend continued into the subsequent decade, up to 2023, with rubber plantations further increasing to 886.98 km² (Table 1). As a result, rubber plantations have become the second largest land use/land cover (LULC) type, after paddy fields.

Overall, there appears to be a significant shift in LULC in the area between 2003 and 2023. The most notable changes include the large increase in para rubber plantation and built-up areas, and the decrease in paddy fields and forest.

Model calibration and validation

The SWAT+ model for the USRB was calibrated and validated using observed flow data of the Kh.74 hydrological station (Figure 1) and the SWAT+ toolbox (Chawanda et al., 2020). The parameters for the paddy field-dominated basin in Thailand were adjusted in accordance with the recommendations of Kakarndee and Kositsakulchai (2020); (Kakarndee & Kositsakulchai, 2021). The most sensitive parameters identified were CN2, SOL_AWC, FLO_MIN, REVAP_MIN, and SOL_BD. The recommended range for the initial SCS runoff curve number (CN2) under moisture condition II varies from 60 to 85, depending on land use types; for example, paddy fields typically range between 70 and 80, while agricultural lands or rubber plantations range between 65 and 75. The available water capacity of the soil layer (SOL_AWC) is generally set between 0.10 and 0.25 mm H_2O/mm soil, with higher values for clay soils and lower values for sandy soils. The water table depth required for return flow (FLO_MIN) is suggested to range from 500 to 1,500 mm, representing typical shallow aquifer conditions in the region. For the water table depth necessary for revap to occur (REVAP_MIN), a value between 50 and 500 mm is suitable to simulate moisture exchange between the saturated and unsaturated zones. Lastly, the bulk density of the soil (SOL_BD) is commonly set between 1.2 and 1.7 g/cm³, depending on soil type, with lighter soils having lower values and denser clay soils having higher values.

Figure 5 shows the model calibration and validation results. The observed flow is represented by the black line, while the simulated flow is shown by the red dashed line. Calibration utilized monthly flow data from 2014 to 2017 and achieved good performance metrics: Nash-Sutcliffe efficiency (NSE) = 0.86, coefficient of determination (R^2) = 0.91, and percent bias (PBIAS) = -24.5%. Validation employed data from 2018 to 2021 and yielded results of NSE = 0.79, R^2 = 0.89, and PBIAS = -36.7%. The high negative PBIAS values in both periods indicate a consistent overestimation of streamflow by the model. This may be attributed to underestimated evapotranspiration or oversimplified groundwater processes, leading to excessive baseflow simulation. To address this, the integration of high-resolution or site-specific climate data, as well as the use of observed evapotranspiration and soil moisture data, is

recommended to improve model reliability. Following the criteria established by Gupta et al. (1999) and Abbaspour et al. (2007) (NSE > 0.75, R^2 > 0.80, and PBIAS < ±25%), the model performance can be classified as good. Consequently, the SWAT+ model demonstrates suitability for further applications within the USRB.

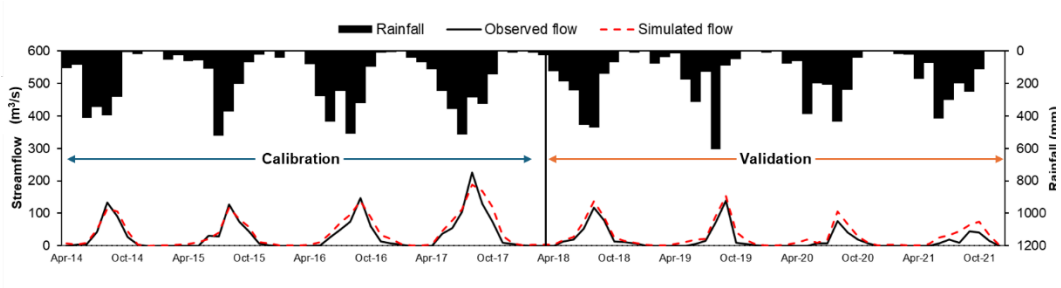

Figure 5 Calibration (2014–2017) and validation (2018–2021) of monthly streamflow

Impacts of LULC change on streamflow

Figure 6 presents the monthly streamflow simulated by SWAT+ for three land-use and land-cover (LULC) periods: LULC 2003 (blue line), LULC 2013 (green line), and LULC 2023 (red line). Wet (May-October) and dry (November-April) period simulations were analyzed separately using the same 5-year baseline dataset (2014-2018). In Table 2 and Figure 6, streamflow patterns in the USRB exhibit minimal change during the dry season (Nov-Apr). In contrast, the wet season (May-Oct) shows a significant increase in streamflow, particularly during flood months (August and September). This variability is exemplified by the high precipitation events observed in 2017.

The analysis used a consistent five-year dataset from 2014 to 2018, focusing on differences in streamflow between wet periods (May to October) and dry periods (November to April). In all three LULC periods, the highest streamflow occurred in August, with values of 131.3 m^3/s, 124.7 m^3/s, and 153.6 m^3/s, respectively, as shown in Table 2.

Table 3 shows the changes in streamflow, with negative values (-) indicating a decrease and positive values (+) indicating an increase, measured in cubic meters per second (m^3/s). Comparing the first decade (2003 to 2013), there was a slight overall decrease in streamflow. The most significant decreases in streamflow occurred in August and September, with a drop of 6.6 m^3/s in August and 5.8 m^3/s in September, as showed in Table 3. This reduction is likely attributed to a slight increase in rice cultivation during these months, which would have resulted in higher water consumption, thus contributing to the overall decline in streamflow levels.

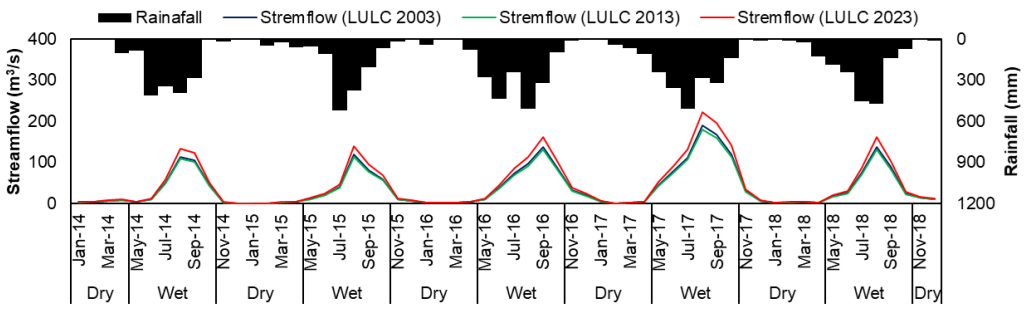

Figure 6 Comparison of monthly streamflow across different LULC periods: 2003, 2013, and 2023

Table 2 Monthly streamflow for three LULC periods during the dry (Oct-Nov) and wet (May-Oct) periods

Period	Month	Streamflow (m³/s)		
		LULC 2003	LULC 2013	LULC 2023
Dry	Jan	2.7	2.5	3.1
	Feb	2.4	2.2	2.8
	Mar	3.5	3.3	4.1
	Apr	4.9	4.7	5.8
Wet	May	17.8	16.9	20.8
	Jun	34.8	33.1	40.7
	Jul	70.1	66.6	82.0
	Aug	131.3	124.7	153.6
	Sep	116.5	110.7	136.3
	Oct	67.1	63.7	78.5
Dry	Nov	18.4	17.4	21.5
	Dec	9.0	8.6	10.6

Table 3 Changes in streamflow for three time periods during the dry (Oct-Nov) and wet (May-Oct) periods

Period	Month	Change of streamflow (m³/s)		
		10 yrs (2003-13)	10 yrs (2013-23)	20 yrs (2003-23)
Dry	Jan	-0.1	+0.5	+0.6
	Feb	-0.1	+0.4	+0.5
Wet	Mar	-0.2	+0.6	+0.8
	Apr	-0.2	+0.8	+1.1
	May	-0.9	+3.0	++3.9
	Jun	-1.7	+5.9	+7.7
	Jul	-3.5	+11.9	+15.4
	Aug	-6.6	+22.3	+28.9
	Sep	-5.8	+19.8	+25.6
	Oct	-3.4	+11.4	+14.8
Dry	Nov	-0.9	+3.1	+4.0
	Dec	-0.5	+1.5	+2.0

Over the past decade (2013–2023), streamflow has shown a notable increase, largely attributed to the reduction of paddy fields resulting from the widespread conversion of agricultural land into para rubber plantations over the past two decades. Traditionally, paddy fields played a crucial role in regulating water flow by serving as natural reservoirs during the rainy season, helping to store excess water and mitigate flooding. However, the decline of these fields has led to significant changes in the region's hydrological condition, especially during periods of heavy rainfall. This transformation is evident in the heightened streamflow rates observed in recent years. Looking at the entire 20-year period (2003–2023), the most significant increase in streamflow during the rainy season occurred in August, with a rise of 28.9 m³/s, followed by September, which saw an increase of 25.6 m³/s, as detailed in Table 3. Table 3 further shows a significant increase in wet-season streamflow from 2013–2023 compared to 2003–2013, particularly between May and October. For instance, streamflow in August rose from -6.6 m³/s to +22.3 m³/s, marking an increase of 28.9 m³/s over 20 years.

While changes in the dry season are minimal, the sharp rise in wet-season streamflow aligns with research on Land Use and Land Cover (LULC) changes. Studies suggest that urbanization and deforestation increase surface runoff and reduce infiltration, as observed in agricultural areas in Thailand (Chotpantarat & Boonkaewwan, 2018). In contrast, large-scale

reforestation efforts, such as those in China's Loess Plateau (Zhou et al., 2013), have been shown to reduce surface runoff, differing from this study's findings. In this study area, the decline of paddy fields, which traditionally functioned as natural retention areas, along with the widespread expansion of para rubber plantations, has reduced the watershed's ability to retain and delay runoff. This has contributed to higher and more rapid streamflow during the rainy season. These trends indicate that LULC changes—likely due to agricultural expansion, urbanization, or deforestation—have driven the increase in wet-season streamflow, highlighting the significant impact of land cover changes on seasonal hydrological patterns.

Conclusions

This research successfully utilized Google Earth Engine (GEE) and SWAT+ modeling to examine the effects of land-use and land-cover change (LUCC) on streamflow in the Upper Songkhram River Basin (USRB), Northeast Thailand. GEE cloud-based platform enabled efficient and accurate LUCC classification (Overall Accuracy: 83-91%, Kappa coefficient: 0.76-0.85). This demonstrates its potential for similar land cover monitoring applications. The study revealed substantial LUCC in the USRB between 2003 and 2023, specifically the expansion of para rubber plantations and built-up areas, besides a decline in paddy fields and forests. he SWAT+ model demonstrated good performance (NSE during calibration/validation: 0.86/0.79, R^2: 0.91/0.89, PBIAS: -24.5%/-36.7%) provides confidence in the simulations used to analyze the impact of LUCC on streamflow. Main parameters adjusted during calibration included Curve Number (CN2), baseflow alpha factor (ALPHA_BF), groundwater delay time (GW_DELAY), and soil hydraulic properties (SOL_K, SOL_AWC), which were optimized based on sensitivity analysis. Calibration results indicated that the model adequately captured streamflow variability. Overall, the observed LUCC patterns within the USRB, especially the conversion of forests and paddy fields, directly contributed to altered streamflow dynamics. It is important to note that users of GEE and SWAT+ should possess adequate expertise to ensure greater accuracy and reliability of the results.

Acknowledgements

The authors gratefully acknowledge the research funding provided by the Department of Farm Mechanics and the Faculty of Agriculture at Kasetsart University, Bangkok, Thailand. This support was essential to the successful completion of this research

References

Abbaspour, K. C., Rouholahnejad, E., Vaghefi, S., Srinivasan, R., Yang, H., & Kløve, B. (2015). A continental-scale hydrology and water quality model for Europe: Calibration and uncertainty of a high-resolution large-scale SWAT model. **Journal of Hydrology**, 524, 733-752.

Abbaspour, K. C., Yang, J., Maximov, I., Siber, R., Bogner, K., Mieleitner, J., Zobrist, J., & Srinivasan, R. (2007). Modelling hydrology and water quality in the pre-alpine/alpine Thur watershed using SWAT. **Journal of Hydrology**, 333(2-4), 413-430.

Alzurqani, S. A., Zurqani, H. A., White, D., Bridges, K., & Jackson, S. (2024). Google Earth Engine application for mapping and monitoring drought patterns and trends: A case study in Arkansas, USA. **Ecological Indicators**, 168, 112759.

Amani, M., Ghorbanian, A., Ahmadi, S. A., Kakooei, M., Moghimi, A., Mirmazloumi, S. M., Moghaddam, S. H. A., Mahdavi, S., Ghahremanloo, M., Parsian, S., Wu, Q., & Brisco, B. (2020). Google Earth Engine Cloud Computing Platform for Remote Sensing Big Data Applications: A Comprehensive Review. **IEEE Journal of Selected Topics in Applied Earth Observations and Remote Sensing**, 13, 5326-5350.

Anderson, J. R., Hardy, E. E., Roach, J. T., & Witmer, R. E. (1976). A land use and land cover classification system for use with remote sensor data. **In Professional Paper**.

Ara, Z., Jha, R., & Quaff, A. R. (2023). **Critical Appraisal of Satellite Data for Land Use/Land Cover Classification and Change Detection: A Review**. Geospatial and Soft Computing Techniques, Singapore.

Arnold, J. G., Srinivasan, R., Muttiah, R. S., & Williams, J. R. (2007). Large Area Hydrologic Modeling and Assessment Part I: Model Development1. **JAWRA Journal of the American Water Resources Association**, 34(1), 73-89.

Bieger, K., Arnold, J. G., Rathjens, H., White, M. J., Bosch, D. D., Allen, P. M., Volk, M., & Srinivasan, R. (2017). Introduction to SWAT+, a completely restructured version of the soil and water assessment tool. **JAWRA Journal of the American Water Resources Association**, 53(1), 115-130.

Breiman, L. (2001). Random Forests. **Machine Learning**, 45(1), 5-32.

Čerkasova, N., White, M., Arnold, J., Bieger, K., Allen, P., Gao, J., Gambone, M., Meki, M., Kiniry, J., & Gassman, P. W. (2023). Field scale SWAT+ modeling of corn and soybean yields for the contiguous United States: National Agroecosystem Model Development. **Agricultural Systems**, 210.

Chawanda, C. (2022). *SWAT+ Toolbox (0.7.6)*. Zenodo. Retrieved from https://zenodo.org/records/6331716

Chawanda, C. J., Arnold, J., Thiery, W., & van Griensven, A. (2020). Mass balance calibration and reservoir representations for large-scale hydrological impact studies using SWAT+. **Climatic change**, 163(3), 1307-1327.

Chotpantarat, S., & Boonkaewwan, S. (2018). Impacts of land-use changes on watershed discharge and water quality in a large intensive agricultural area in Thailand. **Hydrological Sciences Journal**, 63(9), 1386-1407.

Congalton, R. G. (1991). A review of assessing the accuracy of classifications of remotely sensed data. **Remote Sensing of Environment**, 37(1), 35-46.

Gassman, P. W., Reyes, M. R., Green, C. H., & Arnold, J. G. (2007). The Soil and Water Assessment Tool: Historical Development, Applications, and Future Research Directions. **Transactions of the ASABE**, 50(4), 1211-1250.

Gassman, P. W., Sadeghi, A. M., & Srinivasan, R. (2014). Applications of the SWAT Model Special Section: Overview and Insights. **Journal of Environmental Quality**, 43(1), 1-8.

Gorelick, N., Hancher, M., Dixon, M., Ilyushchenko, S., Thau, D., & Moore, R. (2017). Google Earth Engine: Planetary-scale geospatial analysis for everyone. **Remote Sensing of Environment**, 202, 18-27.

Guo, Y., Fang, G., Xu, Y. P., Tian, X., & Xie, J. (2020). Identifying how future climate and land use/cover changes impact streamflow in Xinanjiang Basin, East China. **Science of The Total Environment**, 710, 136275.

Gupta, H. V., Sorooshian, S., & Yapo, P. O. (1999). Status of Automatic Calibration for Hydrologic Models: Comparison with Multilevel Expert Calibration. **Journal of Hydrologic Engineering**, 4(2), 135-143.

Hansen, M. C., Potapov, P. V., Moore, R., Hancher, M., Turubanova, S. A., Tyukavina, A., Thau, D., Stehman, S. V., Goetz, S. J., Loveland, T. R., Kommareddy, A., Egorov, A., Chini, L., Justice, C. O., & Townshend, J. R. (2013). High-resolution global maps of 21st-century forest cover change. **Science**, 342(6160), 850-853.

Her, Y., & Jeong, J. (2018). SWAT+ versus SWAT2012: Comparison of Sub-Daily Urban Runoff Simulations. **Transactions of the ASABE**, 61(4), 1287-1295.

Huang, H., Chen, Y., Clinton, N., Wang, J., Wang, X., Liu, C., Gong, P., Yang, J., Bai, Y., Zheng, Y., & Zhu, Z. (2017). Mapping major land cover dynamics in Beijing using all Landsat images in Google Earth Engine. **Remote Sensing of Environment**, 202, 166-176.

Kadhum, Z. M., Jasim, B. S., & Al-Saedi, A. S. J. (2023). Improving the spectral and spatial resolution of satellite image using geomatics techniques. **AIP Conference Proceedings**, 2776(1), 040011.

Kakarndee, I., & Kositsakulchai, E. (2020). **Comparison between SWAT and SWAT+ for simulating streamflow in a paddy-field-dominated basin, northeast Thailand**. The 13th Thai Society of Agricultural Engineering International Conference (TSAE 2020), 187, 1-9.

Kakarndee, I., & Kositsakulchai, E. (2021). Impact of Climate Change on Water Balance in Lam Siao Basin Using SWAT+ Model. **Thai Socity of Agricultural Engineering Journal**, 29(2), 1-11.

Kim, W., Kanae, S., Agata, Y., & Oki, T. (2005). Simulation of potential impacts of land use/cover changes on surface water fluxes in the Chaophraya river basin, Thailand. **Journal of Geophysical Research: Atmospheres**, 110(D8), 1-10.

Lozano, P. J. J., & Regan, A. (2018). **Land surface satellite remote sensing gap analysis**. Sixth International Conference on Remote Sensing and Geoinformation of the Environment (RSCy2018).

Luo, K., Tao, F., Moiwo, J. P., & Xiao, D. (2016). Attribution of hydrological change in Heihe River Basin to climate and land use change in the past three decades. **Scientific Reports**, 6, 33704.

Mbinya Manetu, W., Momanyi Mironga, J., & Haywood Ondiko, J. (2023). Remote Sensing for Land Resources: A Review on Satellites, Data Availability and Applications. **American Journal of Remote Sensing**, 10(2), 39-49.

Muangthong, S., & Shrestha, S. (2015). Assessment of surface water quality using multivariate statistical techniques: case study of the Nampong River and Songkhram River, Thailand. **Environmental monitoring and assessment**, 187(9), 1-12.

Mutanga, O., & Kumar, L. (2019). Google Earth Engine Applications. **Remote Sensing**, 11(5).

Näschen, K., Diekkrüger, B., Evers, M., Höllermann, B., Steinbach, S., & Thonfeld, F. (2019). The Impact of Land Use/Land Cover Change (LULCC) on Water Resources in a Tropical Catchment in Tanzania under Different Climate Change Scenarios. **Sustainability**, 11(24), 1-11.

Ninad, M. (2024). A Complete Study of Remote Sensing- Sentinel-2 Satellite Data for Land Use / Land Cover (LULC) Analysis. **Panamerican Mathematical Journal**, 35(1s), 231-249.

Peng, J., Liu, T., Chen, J., Li, Z., Ling, Y., De Wulf, A., & De Maeyer, P. (2023). The conflicts of agricultural water supply and demand under climate change in a typical arid land watershed of Central Asia. **Journal of Hydrology: Regional Studies**, 47, 1-16.

Petchprayoon, P., Blanken, P. D., Ekkawatpanit, C., & Hussein, K. (2010). Hydrological impacts of land use/land cover change in a large river basin in central–northern Thailand. **International Journal of Climatology**, 30(13), 1917-1930.

Qi, Y., Zhang, X., & Yin, Q. (2024). Assessing water resource vulnerability based on remote sensing data-enhanced SWAT+ and High-Resolution precipitation data. **Ecological Indicators**, 169.

Sain, S. R. (1996). The Nature of Statistical Learning Theory. **Technometrics**, 38(4), 409-409.

Shelestov, A., Lavreniuk, M., Kussul, N., Novikov, A., & Skakun, S. (2017). Exploring Google Earth Engine Platform for Big Data Processing: Classification of Multi-Temporal Satellite Imagery for Crop Mapping. **Frontiers in Earth Science**, 5(17).

Tamiminia, H., Salehi, B., Mahdianpari, M., Quackenbush, L., Adeli, S., & Brisco, B. (2020). Google Earth Engine for geo-big data applications: A meta-analysis and systematic review. **ISPRS Journal of Photogrammetry and Remote Sensing**, 164, 152-170.

Tyukavina, A., Hansen, M. C., Potapov, P., Parker, D., Okpa, C., Stehman, S. V., Kommareddy, I., & Turubanova, S. (2018). Congo Basin forest loss dominated by increasing smallholder clearing. **Sci Adv**, 4(11), 1-12.

Velastegui-Montoya, A., Montalván-Burbano, N., Carrión-Mero, P., Rivera-Torres, H., Sadeck, L., & Adami, M. (2023). Google Earth Engine: A Global Analysis and Future Trends. **Remote Sensing**, 15(14), 1-30.

Wafdan, L. (2021). **Accuracy Assessment of Land Use/Land Cover Classification Data from Sentinel-2 & ASTER Imagery Interpretation using Unsupervised Classification Algorithm**. Proceeding International Conference on Science and Engineering. (Vol. 4, pp. 229–234). Yogyakarta, Indonesia.

Williams, J. R., Arnold, J. G., Kiniry, J. R., Gassman, P. W., & Green, C. H. (2010). History of model development at Temple, Texas. **Hydrological Sciences Journal**, 53(5), 948-960.

Woo, S. Y., Jung, C. G., Lee, J. W., & Kim, S. J. (2019). Evaluation of Watershed Scale Aquatic Ecosystem Health by SWAT Modeling and Random Forest Technique. **Sustainability**, 11(12).

Wu, J., Yen, H., Arnold, J. G., Yang, Y. C. E., Cai, X., White, M. J., Santhi, C., Miao, C., & Srinivasan, R. (2020). Development of reservoir operation functions in SWAT+ for national environmental assessments. **Journal of Hydrology**, 583. 124556.

Yong, B., Jiang, S., Yuan, F., Liu, X., Singh, V. P., Ren, L., & Yang, X. (2012). Impacts of land use and land cover changes on evapotranspiration and runoff at Shalamulun River watershed, China. **Hydrology Research**, 43(1-2), 23-37.

Younes, A., Ahmad, A., Hanjag, A. D., & Nair, A. M. (2023). Understanding Dynamics of Land Use & Land Cover Change Using GIS & Change Detection Techniques in Tartous, Syria. **European Journal of Geography**, 14(3), 20-41.

Zhang, L., Jiang, Y., Yang, M., Wang, H., Dong, N., Wang, H., Liu, X., Chen, L., & Liu, K. (2022). Quantifying the Impacts of Land Use and Cover Change (LUCC) and Climate Change on Discharge and Sediment Load in the Hunhe River Basin, Liaoning Province, Northeast China. **Water**, 14(5), 1-14.

Zhou, F., Xu, Y., Chen, Y., Xu, C. Y., Gao, Y., & Du, J. (2013). Hydrological response to urbanization at different spatio-temporal scales simulated by coupling of CLUE-S and the SWAT model in the Yangtze River Delta region. **J ournal of Hydrology**, 485(3), 113-125.

Zope, P. E., Eldho, T. I., & Jothiprakash, V. (2014). Impacts of urbanization on flooding of a coastal urban catchment: a case study of Mumbai City, India. **Natural Hazards**, 75(1), 887-908.